reactants via reverse micelles results in a different intramicellar composition than the starting solutions. Gier and Stucky's reported procedure necessitated a pH of 7.4 and proceeded through an amorphous gel into sodalite[6], whereas in the micellar system, there was no immediate formation of an amorphous phase. The reverse micelles are clearly influencing the mixing of the reactants. These micelles diffuse by brownian motion and collisions between them can result in fusion. The time period of existence of dimers is of the order of microseconds[16]. This temporary fusion causes incorporation of zinc and phosphate species in the same micelle, and reactions ensue between them leading to nucleation of the sodalite crystals. The particle-growth data show continuous linear growth, unlike the sigmoid curves observed during nucleation in conventional microporous-material synthesis. The surfactant-surrounded nuclei grow into crystals by incorporating species from other micelles via collisions promoted by diffusion and convection. The crystals remain suspended as long as the thermal brownian diffusive motion balances the gravitational forces. For the 600-nm crystals, we calculate from the Stokes relation[17] a terminal settling velocity of 0.5 cm h^{-1}, which would result in particles settling out in a maximum of 10 hours. Once settled, the crystals lose contact with the nutrient pool and stop growing. Recent work on crystallization of silicalite from clear solutions showed that if the product is removed from the system, nucleation and crystal growth will restart[18]. In our case, sedimentation effectively stops further growth of settled crystals, whereas in solution nucleation and crystal growth continue. This leads to an equilibrated steady-state value of 140 nm for the size of the suspended crystallites. The smaller sizes of the settled crystals recovered after 14 days of reaction (400–500 nm) as compared to the crystals recovered after 4 days (600 nm) arise owing to increasing number of crystals being nucleated with time, resulting in competition and depletion of the nutrient pool.

The most interesting aspect is the morphology of the crystals (Fig. 3). Sodalites typically exhibit morphologies characteristic of their cubic symmetry, which are manifested as cubes and octahedra[19,20]. Several cubes are seen in Fig. 3b. Of more interest, however, are the incomplete cubic crystals seen in Fig. 3*a* and *b*, which exhibit triangular faces, and can be viewed as partially formed cubes, with the (111) or (110) faces stabilized. A diagram of such structures and their connection to the cube is shown in Fig. 4. Crystal growth rates can be strongly influenced by the adsorption of "impurities" on a crystal face[21]. In the present case, as a single {111} and/or {110} face is being manifested, these faces are possibly the sites for preferential binding of the surfactants, and form the original template for nucleation. Thus the sulphonate groups of the AOT at the interface of the reverse micelle align the Zn^{2+} ions along the (111) and/or (110) face that begins the nucleation process. This leads to crystal growth in a layer-by--layer fashion on the {100} faces. It is interesting to note that in a recent study on another zincophosphate crystal of cubic morphology, the crystals exhibited a preferential growth along the (111) face on a zirconium phosphonate substrate[22].

In previous experiments using reverse micelles and vesicles for synthesis of solids, the particle growth was primarily a precipitation process due to supersaturation[13,23]. In the work reported here, the reverse micelles help nucleate the crystals, and micellar interactions enable crystal growth by deposition along specific crystal faces. Evaluation of the features on the growing crystal face as a function of time will provide a better understanding of the mechanism of crystal growth of microporous materials. □

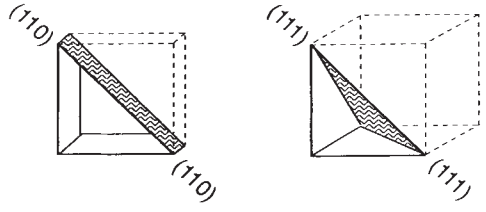

FIG. 4 A schematic presentation of crystal growth of the zincophosphate sodalite by nucleation along the (110) or (111) faces.

Received 6 October 1994; accepted 16 January 1995.

1. Davis, M. E. & Lobo, R. F. *Chem. Mater.* **4,** 756–768 (1992).
2. Wenqin, P., Ueda, S. & Koizumi, M. in *Proc. 7th Int. Zeolite Conf.* 177–184 (Kodanasha Elsevier, Tokyo, 1986).
3. Jacobs, P. A. & Martens, J. A. *Synthesis of High-Silica Aluminosilicate Zeolites* (Elsevier, Amsterdam, 1987).
4. Kresge, C. T., Leonwicz, M. E., Roth, W. J., Vartuli, J. C. & Beck, J. S. *Nature* **359,** 710–712 (1992).
5. Monnier, A. *et al. Science* **261,** 1299–1303 (1993).
6. Gier, T. E. & Stucky, G. D. *Nature* **349,** 508–510 (1991).
7. Nenoff, T. M., Harrison, W. T. A., Gier, T. E. & Stucky, G. D. *J. Am. chem. Soc.* **113,** 378–379 (1991).
8. Gier, T. E., Harrison, W. T. A., Nenoff, T. M. & Stucky, G. D. in *Synthesis of Microporous Materials* Vol. 1 (eds Occelli, M. & Robson, H.) 407–426 (Van Nostrand Reinhold, New York, 1992).
9. Osseo-Asare, K. & Arriagada, F. J. *Colloids Surfaces* **50,** 321–339 (1990).
10. Fendler, J. H. *Chem. Rev.* **87,** 877–899 (1987).
11. Wilcoxon, J. P., Williamson, R. L. & Baughman, R. *J. chem. Phys.* **98,** 9933–9950 (1993).
12. Mann, S. & Williams, R. J. P. *J. chem. Soc., Dalton Trans.* 311–316 (1983).
13. Pileni, M. P. *J. phys. Chem.* **97,** 6981–6973 (1993).
14. Kahlweit, M., Strey, R., Busse, G. *J. phys. Chem.* **94,** 3881–3894 (1990).
15. Kuneida, H. & Shinoda, K. *J. Colloid Interface Sci.* **75,** 601–606 (1980).
16. Fletcher, P. D. I., Howe, A. M. & Robinson, B. H. *J. chem. Soc., Faraday Trans. 1* **83,** 985–1006 (1987).
17. Hunter, R. J. *Foundations of Colloid Science* Vol. 1 49–103 (Clarendon, Oxford, 1993).
18. Twomey, T. A. M., Mackay, M., Kuipers, H. P. C. E. & Thompson, R. W. *Zeolites* **14,** 162–168 (1994).
19. Bibby, D. M. & Dale, M. P. *Nature* **317,** 157–158 (1985).
20. Loades, S. D., Carr, S. W., Gay, D. H. & Rohl, A. L. *J. chem. Soc., chem. Commun.* 1369–1370 (1994).
21. Hartman, P. & Bennema, P. *J. Cryst. Growth* **49,** 145–156 (1980).
22. Feng, S. & Bein, T. *Nature* **368,** 834–836 (1994).
23. Towey, T. F., Khan-Lodhi, A. & Robinson, B. H. *J. chem. Soc., Faraday Trans.* **86,** 3757–3762 (1990).

ACKNOWLEDGEMENTS. We acknowledge discussions with C. Kresge and R. Ansari. This work was supported by NASA.

Variations in atmospheric methane concentration during the Holocene epoch

T. Blunier*, J. Chappellaz†, J. Schwander*, B. Stauffer* & D. Raynaud†

* Physics Institute, University of Bern, Sidlerstrasse 5, CH-3012 Bern, Switzerland
† CNRS Laboratoire de Glaciologie (LGGE), BP 96, 38402 St Martin d'Hères Cedex, Grenoble, France

RECORDS of the variation in atmospheric methane concentration have been obtained from ice cores for the past 1,000 years and for the period 8,000–220,000 yr BP (refs 1–4), but data for the intervening period, spanning most of the present interglacial period (Holocene), are patchy (refs 5–7 and references therein). Here we present a continuous, high-resolution record of atmospheric methane from 8,000 to 1,000 yr BP, from the GRIP ice core in central Greenland. Unlike most other climate proxies from ice cores (such as oxygen isotope composition[8] and electrical conductivity[9]), methane concentrations show significant variations—up to 15%—during the Holocene. We have proposed[1] that variations in the hydrological cycle at low latitudes are the dominant control on past levels of atmospheric methane. This is now supported by the observation that the lowest methane concentrations in our new record occur in the mid-Holocene, when many tropical lakes dried up[10]. The concentration increases during the Late Holocene, probably owing to an increasing contribution from northern wetlands.

Earlier reconstructions of past CH_4 changes from both Greenland and Antarctic ice cores[1,5,7] showed that glacial–interglacial climate changes are accompanied by large variations in atmospheric methane concentration. Recently, detailed results[1] from the GRIP core (Summit, central Greenland; 72° 34′ N, 37° 37′ W; altitude, 3,230 m) revealed that rapid variations in Greenland climate during the last glaciation and deglaciation[8] are reflected in the methane record. Over the past millennium, measurements on the Eurocore ice core (Summit) showed that the CH_4 pre-industrial level fluctuated by ~10%. Although these fluctuations are only partially correlated with climate variations[2], it was concluded that the large variations during and at the end of the last glaciation were mainly linked to changes in the hydrological cycle at low latitudes[1]. Thus atmospheric CH_4 concentration changes in the Holocene epoch are expected to parallel (at least to a certain degree) large-scale climate changes. In particular, it was suggested[10] that there could be another distinct CH_4 decrease in the Middle Holocene when many tropical lakes dried up.

So far, the Holocene has been investigated in detail only for the past millennium[2,4]. For the earlier Holocene, less detailed measurements have been made on various ice cores (refs 5–7 and references therein), but either the scatter of the results was too large or the number of the measurements along one single core too small to allow for a detailed reconstruction of the atmospheric CH_4 concentration. The Early Holocene part of the GRIP core originates partially from a zone of brittle ice. This demands special precautions for the preparation of samples which are fulfilled by allowing the core one year of relaxation and by selecting unbroken core pieces.

The measurements presented have been performed in Bern with a dry extraction technique[2] and in Grenoble with a melting–refreezing method[1]. In both laboratories the extracted air is analysed by gas chromatography. The analytical precision amounts to ±37 and ±20 (2σ) parts per billion by volume (p.p.b.v.) for Grenoble and Bern, respectively[1,2]. Replicate measurements on the same depth levels fit into the estimated analytical precision.

Grenoble measurements give values that are generally ~30 p.p.b.v. lower than those obtained in Bern. Standard-gas intercalibration between the laboratories has shown no difference, but extraction methods have been slightly changed in both laboratories since coherent intercalibrations were obtained[2]. The difference between values obtained by the two laboratories probably reflects the uncertainties in estimating the contamination introduced by the extraction systems, as well as potential fractionation effects during transfer of the gas samples through the extraction lines. In any case, the profiles from the two establishments reveal very similar trends, suggesting a rather stable systematic shift. We homogenized the data sets so that the mean values of overlapping parts agree (constant shift of +15 and −15 p.p.b.v. for Grenoble and Bern, respectively). This rather arbitrary correction does not affect the CH_4 Holocene trends depicted by our record. The new measurements agree within the error limits with our previous measurements from Eurocore[2].

The timescale for the ice is provided by the GRIP glaciological model[8], modified such that the best fit on Holocene stratigraphic markers is obtained (S. Johnsen, personal communication). At Summit, the air-enclosure process takes place ~70 m below the surface under present-day conditions. Thus the air in the bubbles is younger than the surrounding ice. Today's age difference amounts to[11] ~210 yr. Because of the diffusive mixing in the firn and the gradual enclosure process, the air in the bubbles has not a discrete age but rather an age distribution with a standard deviation of ~7 yr. Climate conditions over the Holocene at the GRIP site did not vary significantly[8]. Therefore the past air–ice difference in age, calculated with a semi-empirical model of firn densification[12], varies little (between 200 and 240 yr) for the depth levels presented here.

Samples from a total of 92 depth levels were analysed. The samples were distributed alternately between the two laboratories. The mean difference between depth levels is 13 m (minimum 3 m, maximum 36 m) corresponding to a mean time resolution of 85 yr (range from 29 to 228 yr).

The atmospheric methane concentration is plotted against age and depth together with the GRIP isotopic record[8] in Fig. 1. The trends depicted by the two laboratories agree remarkably well except in the time interval 7–8 kyr BP, corresponding to 1,220–1,320 m depth, where the results from Bern are (after the +15/−15 p.p.b.v. correction) up to 50 p.p.b.v. higher than the Grenoble ones, combined with unusually high scattering. Some ice samples from this interval have been exchanged between the laboratories for re-measurement. We find again that the results from Bern are unusually high compared to results from Grenoble. We note that this effect occurs in a depth where air bubbles end their transformation into air-hydrates, due to the increasing pressure with depth (S. Kipfstuhl, personal communi-

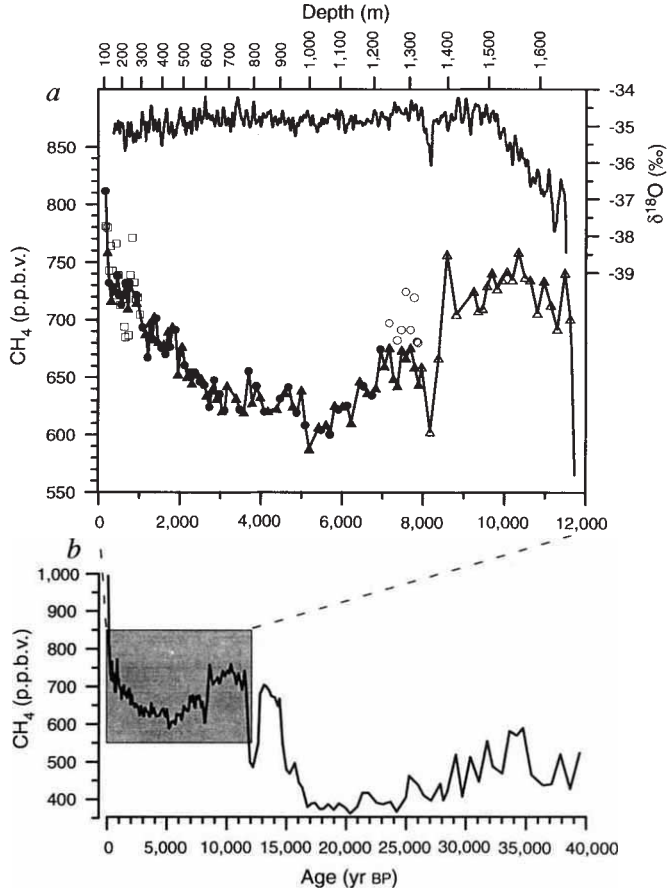

FIG. 1 *a*, Mean atmospheric methane concentrations from the Greenland ice-cores GRIP (ref. 1 and this work) and Eurocore[2] over the past 40,000 yr (mean values for each depth level). Note that the plot ends at 1,000 p.p.b.v., whereas today's concentration is ~1,700 p.p.b.v.; the spike at 800 yr BP originates from the more detailed Eurocore record. *b*, Expanded-scale plot of data for the past 12,000 yr. Top trace, isotopic record[8] smoothed by a 11-m guassian low-pass filter based on 0.55-m data sets. Bottom trace, methane record: filled circles and filled triangles mean results from Bern and Grenoble respectively (this work); open circles, measurements affected by air-hydrates (see text); open triangles, results from ref. 1; open squares, mean values from the Eurocore record[2]. Note that the timescale is in calender years; Bern results are lowered by 15 p.p.b.v., whereas results from Grenoble and ref. 1 are raised by 15 p.p.b.v., to homogenize the records.

cation). As the dry extraction used in Bern leads to higher concentrations than the Grenoble wet extraction, this suggests that at these depths, the bubbles, easily opened by the dry extraction, contain an over-proportional amount of methane versus nitrogen and oxygen, and that a significant part of air-hydrates resist the crushing. This hypothesis is supported by the observation of decreasing efficiency (by ~10%) of the dry-extraction process in the corresponding depth range. Unfortunately, the dry-extraction efficiency cannot be quantified accurately enough to allow a correction to the measured concentrations. We therefore consider in this depth range only the results of the wet extraction, where most of the gas stored in bubbles and air-hydrates is obtained, as a signal of the atmospheric CH_4 concentration.

The most striking feature of the CH_4 profile plotted in Fig. 1 is the observation of significant variations throughout the Holocene epoch. The highest concentrations are found during the first 2,000 yr of the interglacial, and then not before the past millennium; during the Middle Holocene, concentrations are lower by as much as 100 p.p.b.v.. Such general features of the CH_4 record have no analogy in the GRIP climate isotopic record. In addition, over most of the Holocene, the background CH_4 level stands more around 650 p.p.b.v. than at the commonly accepted 700 p.p.b.v. interglacial level (which is mainly based on concentration measurements from the recent millennium). Our data is in accordance with the trends noted in previously published data[5–7]. However, the uncertainty in dating and the scatter of published records precludes a detailed comparison.

Going forward in time, from 11.5 to 8.5 kyr BP, CH_4 concentrations fluctuate slightly around a mean 725-p.p.b.v. level; then a sharp decrease to 600 p.p.b.v. happens[1] at 8.2 kyr BP, followed by an increase towards a mean level of 670 p.p.b.v.. Between 7 and 5.2 kyr BP, methane decreases again and reaches its lowest Holocene concentration. The following increase occurs in steps. A first rapid increase of 40 p.p.b.v. takes place within ~200 yr. During the following 2 kyr, concentrations stay constant at ~630 p.p.b.v.. This plateau is followed by an increase until ~1,000 yr BP, where methane reaches its Greenland pre-industrial 730-p.p.b.v. level, as found in other Greenland records[2,4].

The abrupt fall and subsequent rise in methane at 8.2 kyr is paralleled by a similar feature in the isotope record. The two signals are synchronous within our time resolution, that is, ~100 yr. As the CH_4 oscillation has its origin in large-scale climate shifts, whereas the isotope signal is of a more regional character, a correlation between the two signals indicates that the climate event at 8.2 kyr BP affected a significant part of at least the Northern Hemisphere.

We discussed previously[1] the potential mechanisms driving past natural CH_4 changes, in particular during the sequence of the last deglaciation. Three potential scenarios could explain the glacial–interglacial CH_4 doubling: clathrate outgassing, decrease of the tropospheric oxidative capacity, and increase in global wetland extent. We favoured the large extension of low-latitude wetlands, depicted by other palaeoclimate data as the most probable scenario. We still exclude the first two scenarios as the main explanations of the Holocene CH_4 variations, as discussed below.

First, clathrate outgassing: the Early Holocene was the time of the large retreat of the Laurentide ice sheet (until 7 kyr BP), which should have led, according to the clathrate hypothesis[13], to a large transient increase in the methane concentration from catastrophic burst events potentially occurring in permafrost regions and/or in continental shelves. Our detailed profile shows no evidence for the occurrence of this kind of event. Such absence cannot be due to the air-trapping process, which could only smooth variations of less than ~20 yr duration under Holocene conditions. However, we do not rule out continuous clathrate decomposition (from melting permafrost) as a methane source after the deglaciation. But the weak temperature variations together with source estimates for a global warming scenario[14] suggest that this source of CH_4 was relatively small in the later Holocene.

Second, changes in the oxidative capacity of the atmosphere: there is a consensus that changes in the OH concentration were not the driving factor for the CH_4 increase, either from the Last Glacial Maximum to the pre-industrial Holocene, or from the pre-industrial Holocene to today[15]. Because the Holocene is, on a global average, a stable climate period, we assume that parameters expected to affect the OH level independently from CH_4 itself (NO_x, CO) stayed fairly constant and were thus not a primary factor for changes in the methane concentration.

We cannot exclude the possibility that changes in soil uptake of methane may have exhibited a minor effect on atmospheric methane during the Holocene. But soil sink is an order of magnitude smaller than emissions from wetlands[16], so we feel that any effect of this sort would be negligible. In view of these considerations, and for the reasons below, we conclude that the Holocene methane record presented here reinforces the idea that low-latitude wetlands exert the main controlling influence on atmospheric methane.

Conditions were not suitable for wetland formation after the deglaciation in today's main source regions[17] at high northern latitudes. Western Canada[18] and Alaska[19], as well as Scandinavia[20] (until around 8 kyr BP), were generally dry during the Early Holocene; in central Canada[21], major peat formation started only after 7 kyr BP. (Note that all the dates of palaeodata given here are corrected to calendar years). In contrast, observations from various regions, (including the Nile delta[22], India[23], Brazil[24], the Sahel and Sahara, Tibet and China[25]) suggest that at low latitudes, the Early Holocene period was the wettest time of the present interglacial.

The episode of low methane concentration at 8.2 kyr coincides with an episode of drought in tropical Africa[26–28] and Tibet[29]. The drought episode around 8.2 kyr BP might have been even more severe than during the Younger Dryas in some regions[26]. The effect on atmospheric methane is possibly counterbalanced to a certain extent by an expansion of wetlands in the Russian plain[30] and Scandinavia[31].

Low-latitude climate became drier[10] after 5.7 kyr BP. The CH_4 concentration minimum between 5.7 and 5.2 kyr BP is consistent with the maximum aridity at low latitudes[10].

We now consider the methane trends since 5.2 kyr BP. The relative role of low- and high-latitude wetlands seems to have changed since this time; indeed, low latitudes experienced increasingly arid conditions, particularly[25] since 3 kyr BP. On the other hand, the peat growth rate in Canada[21] and Sweden[31], as well as humidity in Alaska[19], significantly increased from 3 to 1 kyr BP. Furthermore, high peat formation rates are reported for the period between 5 and 1 kyr BP in the Fore-Ural[30]. Such Late Holocene peat development in today's biggest wetlands is a good candidate for the cause of the CH_4 concentration increase observed at that time. Overall, methane is probably a good indicator for the global wetland extent; even so, the concentration information by itself does not allow us to quantify the relative importance of high- and low-latitude wetlands. Such quantification could be achieved by performing a similar study on Antarctic ice, using the Greenland/Antarctic CH_4 concentration difference[32] which is directly related to the high-/low-latitude methane emission ratio. The well defined CH_4 variations during the Holocene will also be useful for temporal correlation of the Holocene parts of ice cores. □

Received 4 October 1994; accepted 30 January 1995.

1. Chappellaz, J. *et al. Nature* **366,** 443–445 (1993).
2. Blunier, T. *et al. Geophys. Res. Lett.* **20,** 2219–2222 (1993).
3. Jouzel, J. *et al. Nature* **364,** 407–412 (1993).
4. Nakazawa, T. *et al. Geophys. Res. Lett.* **20,** 943–946 (1993).
5. Chappellaz, J. *et al. Nature* **345,** 127–131 (1990).
6. Stauffer, B., Lochbronner, E., Oeschger, H. & Schwander, J. *Nature* **332,** 812–814 (1988).
7. Machida, T. thesis, Tohoku Univ. (1992).
8. Dansgaard, W. *et al. Nature* **364,** 218–220 (1993).
9. Taylor, K. C. *et al. Nature* **366,** 549–552 (1993).

10. Street-Perrott, F. A. *Nature* **366,** 411–412 (1993).
11. Schwander, J. *et al. J. geophys. Res.* **98,** 2831–2838 (1993).
12. Barnola, J. M., Pimienta, P., Raynaud, D. & Korotkevich, Y. S. *Tellus* **43B,** 83–90 (1991).
13. Nisbet, E. G. *J. geohys. Res.* **97,** 12859–12867 (1992).
14. Moraes, F. & Khalil, M. A. K. *Chemosphere* **26,** 295–607 (1993).
15. Thompson, A. M., Chappellaz, J. A., Fung, I. Y. & Kucsera, T. L. *Tellus* **45B,** 242–257 (1993).
16. Chappellaz, J. A., Fung, I. Y. & Thompson, A. M. *Tellus* **45B,** 228–241 (1993).
17. Fung, I. *et al. J. geophys. Res.* **96,** 13033–13065 (1991).
18. Ritchie, J. C. & Harrison, S. P. in *Global Climates since the Last Glacial Maximum* (eds Wright, H. E. Jr., *et al.*) 401–414 (Univ. Minnesota Press, Minneapolis, 1993).
19. Heusser, C. J., Heusser, L. E. & Peteet, D. M. *Nature* **315,** 485–487 (1985).
20. Harrison, S. P., Prentice, I. C. & Guiot, J. *Clim. Dyn.* **8,** 189–200 (1993).
21. Zoltai, S. C. & Vitt, D. H. *Quat. Res.* **33,** 231–240 (1990).
22. Petit-Maire, N., Fontugne, M. & Rouland, C. *Palaeogeogr. Palaeoclimatol. Palaeoecol.* **86,** 197–204 (1991).
23. Sukumar, R., Ramesh, R., Pant, R. K. & Rajagopalan, G. *Nature* **364,** 703–706 (1993).
24. Ledru, M.-P. *Quat. Res.* **39,** 90–98 (1993).
25. Petit-Maire, N. in *Global Precipitation and Climate Change* (eds Desbois, M. & Desalmand, F.) 3–26 (NATO ASI Ser. I, Vol. 26, Springer, Dordrecht, 1994).
26. Street-Perrott, F. A. & Roberts, N. in *Variations in the Global Water Budget* (eds Street-Perrott, A., Beran. M. & Ratliffe, R.) 331–345 (Reidel, Dordrecht, 1983).
27. Street-Perrott, F. A. & Perrott, R. A. *Nature* **343,** 607–612 (1990).
28. Magaritz, M. *Clim. Change* **24,** 179–185 (1993).
29. Van Campo, E. & Gasse, F. *Quat. Res.* **39,** 300–313 (1993).
30. Latypova, E. K. & Yakheemovich, B. L. *Radiocarbon* **35,** 441–447 (1993).
31. Franzên, L. G. *Ambio* **23,** 300–308 (1994).
32. Rasmussen, R. A. & Khalil, M. A. K. *J. geophys. Res.* **89,** 11599–11605 (1984).

ACKNOWLEDGEMENTS. We thank the GRIP participants for their fieldwork, S. Johnsen for the ice dating, J.-M. Barnola for help with the densification model, S. Kipfstuhl for unpublished information on air-hydrates and A. Neftel for discussion. This work is a contribution to the Greenland Ice-core Project (GRIP) which was coordinated and supported by the European Science Foundation. We thank the national funding organisations in Belgium, Denmark, France, Germany, Iceland, Italy, Switzerland and the UK, together with the XII Directorate of CEC and the University of Bern.

Evidence for Tibetan plateau uplift before 14 Myr ago from a new minimum age for east–west extension

Margaret Coleman & Kip Hodges

Department of Earth, Atmospheric, and Planetary Sciences, 54-1116, Massachusetts Institute of Technology, Cambridge, Massachusetts 02139, USA

IMPORTANT **changes in South Asian climate occurred in the Late Miocene epoch (~8 Myr ago)[1,2], and these have been attributed by some researchers to uplift of the Tibetan plateau at about the same time[3–5]. Unfortunately, this link has been difficult to test because the timing of plateau uplift remains poorly constrained by independent evidence. One way to determine the minimum age of uplift is to establish the initiation age of the north-striking normal fault systems in southern Tibet that are widely regarded[6–10] as being related to gravitational collapse of the Tibetan plateau. Here we report an $^{40}Ar/^{39}Ar$ age of ~14 Myr for hydrothermal mica from an extensional fracture belonging to such a fault system in north-central Nepal. This age implies that east–west extension began before ~14 Myr ago in at least some parts of the Tibetan plateau, suggesting that the plateau attained its high mean elevation well before Late Miocene time.**

The tectonic evolution of the Himalayas and Tibet since the Palaeogene collision between India and Asia has been controlled by three classes of deformational structures. The most obvious features are east-striking, north-dipping thrust fault systems and subordinate folds related to shortening and crustal thickening. Some of these, such as the Neogene Main Central and Main Boundary thrust systems, have been traced for hundreds of kilometres parallel to the strike of the orogen (Fig. 1)[11,12]. The second class of structures includes east-striking, north-dipping normal faults of the South Tibetan detachment system[13]. Developed near the crest of the Himalayas along the southern margin of the Tibetan plateau, these Late Oligocene–Pliocene extensional structures are thought to have moved in concert with contractional faults such as those of the Main Central thrust system in order to moderate high topographical and crustal-thickness gradients arising from the India–Asia convergence[14,15]. Active tectonics of the southern Tibetan plateau are characterized by east–west extension on a third class of structures: north-striking, east- and west-dipping normal faults and related strike-slip features (Fig. 1)[6,7]. Based on the results of numerical experiments on the dynamics of continental plateau uplift, there is general agreement that east–west extension in Tibet was triggered by elevation of the plateau to the point when topography-related extensional stresses exceeded compressional stresses related to continent–continent collision[5,6–10].

Most estimates of the time at which east–west extension began, and thus the minimum age of the plateau attaining its high mean elevation if conventional wisdom proves correct, have been based on chronostratigraphic data for extensional basin deposits related to the second and third classes of structures near the southern margin of the plateau. The most extensively studied Neogene sedimentary sequence in this area is found in the Thakkhola and Giyrong grabens (Fig. 1). Both are characterized by a lower section of fluvial and lacustrine strata separated from an upper fanglomerate section by an angular unconformity[16,17]. Palaeontological and palaeomagnetic data suggest that units found beneath the unconformities range in age from Late Miocene to Early Pliocene[18–20]. The structural setting of the basins in which these rocks were deposited is poorly understood, but the basal units found within the Thakkhola graben overlap NNE-striking extensional faults[17], suggesting that east–west extension may have started before Late Miocene basin sedimentation. There is no question that units above the unconformity were deposited synchronously with the opening of north-trending grabens[17,18]. Palaeomagnetic investigations of these strata indicate Late Pliocene and younger ages. The lack of ambiguity associated with assigning a structural setting to these deposits prompted some researchers[8,18] to postulate a 5–2 Myr age for the inception of east–west extension. More recently, structural and geochronological studies along the western flank of the Yangbajian graben (Fig. 1) suggest that east–west extension in at least one part of the plateau began 11–5 Myr ago[21,22].

Our new constraints on the age of this phase of extension are derived from current studies of the structural evolution of the Annapurna range of north-central Nepal, east of the Thakkhola graben (Fig. 2). The extensional faults that are overlapped by basal units of the Thakkhola Neogene sequence are part of a regionally important family of NNE-striking normal faults with minor displacements that disrupt Palaeozoic and Mesozoic bedrock stratigraphy for ~40 km to the east of the Thakkhola graben[23–25]; we will refer to these structures, together with the syndepositional faults found in the graben, as the Thakkhola fault system. Faults of this system are confined to the region north of the high peaks of the Himalaya, structurally above the lowermost shear zones of the South Tibetan detachment system[25,26].

Our study has focused on some of the easternmost structures of the Thakkhola fault system in the northern part of the Marsyandi river valley (Fig. 2). The most significant of these are normal faults developed in essentially unmetamorphosed Palaeozoic and Mesozoic rocks. They strike N20°E–N40°E and dip 45–60° northwest, similar in orientation to bounding faults of the Thakkhola graben, although we consider them to be older and related to the earliest stages of east–west extension. Striae on exposed fault surfaces are oriented N90°E ± 10°. Kinematic indicators, including slickenside surface characteristics and orientations of extensional fractures within discrete fault zones, demonstrate that displacement was primarily hanging wall down to the WNW. These oldest and easternmost faults of the Thakkhola system cut mylonitic fabrics related to structurally high shear zones of the South Tibetan detachment system, and are